Article

Free Radical Photopolymerization and 3D Printing Using Newly Developed Dyes: Indane-1,3-Dione and 1*H*-Cyclopentanaphthalene-1,3-Dione Derivatives as Photoinitiators in Three-Component Systems

Ke Sun [1,2], **Corentin Pigot** [3] , **Hong Chen** [1,2], **Malek Nechab** [3], **Didier Gigmes** [3],
Fabrice Morlet-Savary [1,2], **Bernadette Graff** [1,2], **Shaohui Liu** [1,2], **Pu Xiao** [4,*], **Frédéric Dumur** [3,*]
and **Jacques Lalevée** [1,2,*]

[1] Université de Haute-Alsace, CNRS, IS2M UMR 7361, F-68100 Mulhouse, France;
   sunke712531@163.com (K.S.); hchen2017@sinano.ac.cn (H.C.); fabrice.morlet-savary@uha.fr (F.M.-S.);
   bernadette.graff@uha.fr (B.G.); shliu2015@163.com (S.L.)
[2] Université de Strasbourg, 67000 Strasbourg, France
[3] Aix Marseille Université, CNRS, ICR UMR 7273, F-13397 Marseille, France; pigotcorentin2@gmail.com (C.P.);
   malek.nechab@univ-amu.fr (M.N.); didier.gigmes@univ-amu.fr (D.G.)
[4] Research School of Chemistry, Australian National University, Canberra ACT 2601, Australia
* Correspondence: pu.xiao@anu.edu.au (P.X.); frederic.dumur@univ-amu.fr (F.D.);
   jacques.lalevee@uha.fr (J.L.)

check for updates

Abstract: The design of photoinitiating systems with excellent photochemical reactivities at 405nm LED is one of the obstacles to efficiently promote free radical polymerization in mild conditions (e.g., low light intensity, under air). Here, our actual search for new multicomponent photoinitiating systems at 405nm LED prompts us to develop new dyes based on push–pull structures. In the present paper, we chose two series of new dyes which possess indane-1,3-dione and 1*H*-cyclopenta naphthalene-1,3-dione groups as the electron-withdrawing groups, since they have the great potential to behave as sensitive and remarkable photoinitiators in vat photopolymerization/3D printing. When incorporated with a tertiary amine (ethyl dimethylaminobenzoate EDB, used as electron/hydrogen donor) and an iodonium salt (used as electron acceptor) as the three-component photoinitiating systems (PISs), and among a series of 21 dyes, 10 of them could efficiently promote the free radical photopolymerization of acrylates. Interestingly, steady state photolysis experiments revealed different behaviors of the dyes. Fluorescence experiments and free energy change calculations for redox processes were also carried out to investigate the relevant chemical mechanisms. Additionally, the formation of radicals from the investigated PISs was clearly observed by electron spin resonance (ESR) spin-trapping experiments. Finally, stereoscopic 3D patterns were successfully fabricated by the laser writing technique. In this work, the use of push–pull dyes based on the naphthalene scaffold as photoinitiators of polymerization is reported for the first time in a systematic study aiming at investigating the structure–performance relationship for irradiation carried out at 405 nm. By carefully selecting the electron donors used in the two series of push–pull dyes, novel and high-performance photoinitiating systems operating at 405 nm are thus proposed.

Keywords: push–pull dye; free radical polymerization; three-component system; LED; 3D printing

1. Introduction

Photopolymerization under visible light and low light intensity is an active research field still requiring the optimization of the chemical structures of photoinitiators [1–12]. With the aim of

improving the polymerization efficiency, several parameters such as the light absorption properties (i.e., the molar extinction coefficient), the excited state lifetime, the redox properties and the energy levels, the photochemical stability or the easiness of synthesis have to be considered as the main parameters governing the reactivity [13–17]. Notably, by increasing the molar extinction coefficients of photoinitiators, the quantity of the compound introduced into the photocurable resin can be drastically lowered while maintaining a constant absorption. This point is of crucial interest, as the extractability and the migratability of photoinitiators within the polymer films can be a major issue for numerous applications such as food packaging [18,19] or the design of biocompatible materials or safety equipment [20–23]. Parallel to the absorption, the excited state lifetime is another point to consider and an elongation of this latter is beneficial by providing more time for the photoinitiator to react with the different additives [24–26]. For an improved reactivity, long-living excited state lifetimes are not sufficient and redox properties adapted with those of the additives are also required in order the redox reaction to proceed [27,28]. As abovementioned, visible light photopolymerization make use of dyes strongly absorbing in the visible range, and the color resulting from the photoinitiator in the polymer film can also be a major issue, especially when colorless coatings are desired. To date, photoinitiators capable to bleach during light irradiation are still scarce so that a great deal of efforts is currently developed by numerous research groups in order to access to these highly desired structures [29–37]. To this end, the development of visible light photoinitiators is also highly researched as the absorption of photoinitiators governs the choice of the irradiation sources and therefore the light penetration [38]. By using long irradiation wavelengths, the polymerization of thick samples and the access to composites is rendered possible, contrarily to the traditional UV photopolymerization for which the polymerization of only thin samples is possible due to a limited light penetration at short wavelength [39]. With regards to these different challenges (light penetration, excited state lifetimes, bleaching properties, molar extinction coefficients), the development of visible light photoinitiators is an active research field imposing new structures to be tested.

Concerning the enhancement of the light absorption properties, the most straightforward route undoubtedly consists in developing dyes with a strong electronic delocalization resulting from the separation of the electron donor from the electron acceptors [40]. This strategy can be easily developed with push–pull dyes comprising an electron donor connected to an electron acceptor by mean of a π-conjugated or a nonconjugated spacer [41,42]. By improving the electron-donating ability of the electron releasing group or the electron-accepting ability of the electron withdrawing group, the position of the charge transfer band located in the visible region can be efficiently tuned. Parallel to this first tool, elongation of the π-conjugated spacer can red-shift the position of this band while improving the molar extinction coefficient, offering another efficient tool to finely tune the absorption of the push–pull dyes [43]. Benefiting from these different advantages, dyes with excellent visible light absorption properties extending over the whole visible range and with high molar extinction coefficients have been developed, attracting the attention of photopolymerists [44–47].

Even if a wide range of chromophores based on push–pull structures were already investigated in photopolymerization [48–53], there is still a challenge to develop very reactive structures capable to efficiently initiate a polymerization in mild conditions (low light intensity and under air). Considering that for a given electron donor, the electron-withdrawing ability of the acceptor can be greatly improved by extending the polyaromaticity of the electron-withdrawing moiety, the extended version of a well-known electron acceptor, namely indane-1,3-dione, has been prepared and used to design a series of push–pull dyes [43]. To evidence the benefits of this extension of aromaticity, a comparison between dyes comprising 1*H*-cyclopentanaphthalene-1,3-dione or the well-known indane-1,3-dione has been established.

In this work, two series of dyes with a broad absorption extending over the visible range have been examined for the first time as photoinitiators of polymerization (Scheme 1). More specifically, their polymerization initiating ability will be investigated @405 nm as this wavelength is the reference one in 3D printing. Moreover, the dyes are characterized by different maximum absorption wavelengths,

hence, the comparison of their efficiency for a same wavelength (405nm) will allow a comparison of their performance.

Noticeably, examples of dyes based on 1*H*-cyclopentanaphthalene-1,3-dione are extremely scarce in literature [42,54–57], evidencing the interest and the novelty of the structures proposed in this work. Interestingly, their good light absorption properties @405 nm were anticipated by theoretical calculations and molecular design. The twenty-one dyes reported in this work address several issues concerning the design of photoinitiators. Notably, the different dyes could be prepared using one of the simplest reactions known in organic chemistry, namely, the Knoevenagel reaction which was reported for the first time in 1896 [58]. As for specificity, the concepts of Green chemistry could also be applied. Thus, ethanol could be used as a safe solvent and no expensive transition metal complexes are required to condense the aldehyde onto the activated methylene groups of the different electron acceptors. Parallel to this, the different dyes **1–21** reported in this work could be prepared in high reaction yields (ranging between 74 and 94% yields), without extensive purification processes since all dyes precipitated in ethanol after reaction. A simple filtration was sufficient to get the different molecules in pure form. This last point is of crucial importance as the filtration is the cheapest and the easiest purification process existing to date, and this type of purification can be easily transposed in industry. Parallel to this, the high reaction yields and the possibility to use Green solvents for the synthesis and the subsequent workup make these dyes exceptional candidates for photoinitiation with regards to the procedure used to access to these structures. The twenty-one dyes are also soluble in most of the common organic solvents, ranging from apolar solvents such as alkanes to highly polar solvents such as *N,N*-dimethylformamide (DMF), dimethylsulfoxide (DMSO), or *N,N*-dimethyacetamide (DMA). Thus, a good solubility in resins is thus ensured. Indeed, the solubility of dyes within the photocurable resins also governs their ability to initiate a polymerization process and numerous examples of dyes with remarkable molar extinction coefficients, long-living excited state lifetime and appropriate redox properties could never initiate a polymerization due to their insolubility in resins [59–68]. Interestingly, the twenty-one dyes reported in this work are used for the first time in photoinitiating systems (PISs) combining a tertiary amine, ethyl dimethylaminobenzoate (EDB), as the electronic donor and an iodonium salt (acting as the electron acceptor) to promote the photopolymerization of benchmark acrylate monomers (see Scheme 2). Among all dyes, some of them showed high final monomer conversions and remarkable photoinitiating abilities. Parallel to the monitoring of the polymerization kinetics, photolysis experiments were carried out to characterize the excited state reactivity of the different dyes. Photochemical mechanism involved in the polymerization process was also studied in detail by steady state fluorescence quenching and electron spin resonance (ESR) experiments. The redox properties as well as the free radical generation are also discussed. Finally, to evidence the interest of these new structures, 3D printing experiments were carried out with the newly proposed photoinitiating systems, and some 3D patterns with gradient resolutions were successfully fabricated.

Series A
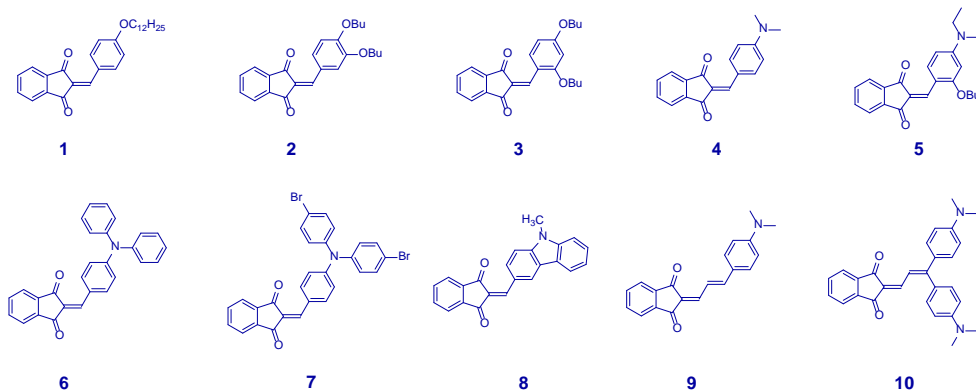
Series B
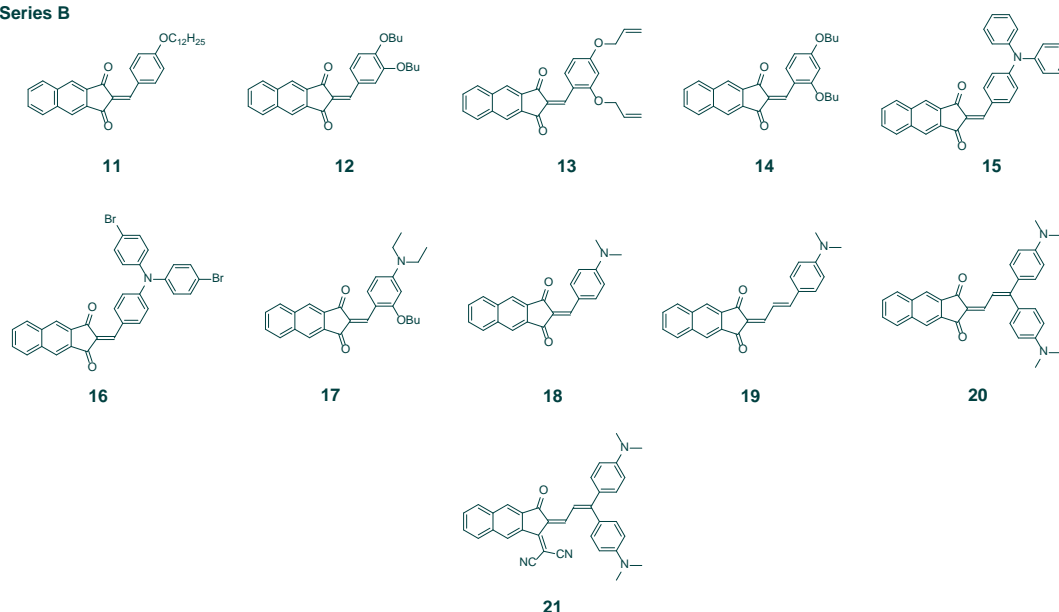
Scheme 1. Chemical structures of dyes **1–21** examined in this study: (**a**) indane-1,3-dione and (**b**) 1*H*-cyclopentanaphthalene-1,3-dione series.
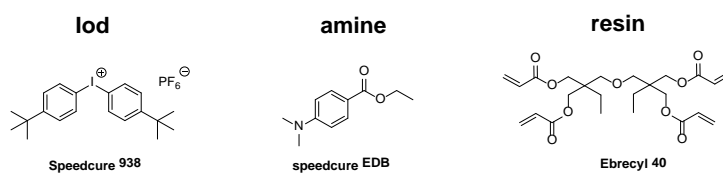
Scheme 2. Chemical structures of the iodonium salt (Iod; Speedcure 938), the amine (ethyl dimethylaminobenzoate (EDB); Speedcure EDB) and the functional benchmark monomer (Ebecryl 40).

2. Results

Photopolymerization Kinetics for the Proposed Dyes in Three-Component Photoinitiating Systems

For the polymerization of the acrylate monomer Ebecryl 40, the photoinitiation abilities of the two series of dye-based PISs (from dye **1** to **21**) were investigated using real-time Fourier transform infrared spectroscopy (RT-FTIR) within the same LED irradiation time (400s) at room temperature, as shown in Figure 1. First, all dyes (**1–21**) were tested as photoinitiators in two-component systems dye/Iod (0.1%/2%), but none of the resulting photoinitiating systems could provide final monomer conversions exceeding 40%, which is extremely low for this acrylate monomer. Therefore, due to the lack of reactivity,

the same dyes were tested in new conditions, in three component photoinitiating systems in which an amine was added to the former dye/Iod systems. The specific polymerization of the two-component PIS Iod/amine without dyes is also given in Figure 1 for comparison and defined as the curve 0. As depicted in the Figure 1, typical acrylate function conversion vs irradiation time profiles indicate that the presence of the dyes is essential to promote the free radical photopolymerization process, based on the comparison established with the Iod/amine two-component systems. As exceptions, for dyes **6**, **11** and **18**, the three-component systems seem to be less efficient than the Iod/amine system (curve 0). In the specific case of dyes **5** and **17**, the two dyes proved to efficiently promote the photopolymerization of Ebecryl 40 and the highest conversions and fastest polymerization processes were obtained with these two dyes. Beyond 90% of final reactive function conversions were attained within 50 s. Interestingly, the two dyes have similar chemical structures, except dye **17** possesses an additional aromatic ring compared to dye **5**. Additionally, an irreversible photobleaching process was evidenced with dye **5** during the photopolymerization process upon irradiation with the LED@405nm, which was not observed for the elongated version of dye **5**, namely dye **17**.
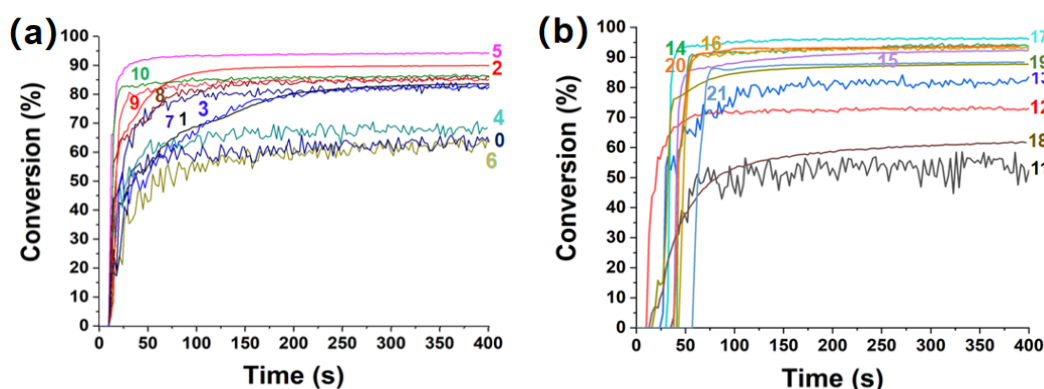

Figure 1. Photopolymerization profiles of Ebecryl 40 (conversion rate of C=C bonds vs irradiation time) initiated by iodonium (Iod) and amine (EDB) upon exposure to LED@405nm under air in the presence of dyes **1**–**21** for curves 1–10 (**a**) and 11–21 (**b**) at the same weight ratio: dye:Iod:amine = 0.1%:2%:2% in Ebecryl 40; the curve number indicated the investigated dye. The reference curve without dye is curve 0 for Iod:amine = 2%:2%. The irradiation starts for t = 10 s.

On the other hand, for all the other dyes, several excellent polymerization profiles were also obtained still upon irradiation with a LED@405nm. Among all dyes, ten of them including the two dyes **5** and **17** (gathered in Table 1) furnished high final conversions beyond 80% and short polymerization times (the polymerization being ended within 50 s). All data concerning the polymerization of Ebecryl 40 are summarized in the Table 1. Compared to these 10 dyes, all the other dyes were less efficient to initiate photopolymerization processes.

Table 1. Summary of the final acrylate function conversions (FCs) at 405 nm for Ebecryl 40 using three-component photoinitiating systems: dyes (0.1%, w/w), iodonium salt (Speedcure 938, 2%, w/w) and amine (Speedcure EDB, 2%, w/w).

Dye	**5**	**9**	**10**	**14**	**15**
FCs	93%	82%	84%	92%	90%
Dye	**16**	**17**	**19**	**20**	**21**
FCs	92%	95%	85%	91%	86%

Overall, in the course of our investigations, dyes **2**, **5**, **14**, **16**, **17** and **20** have been identified as the most promising candidates in terms of final monomer conversions and polymerization rates. The polymerization rates are especially remarkable for dyes **5**, **14**, **16**, **17** and **20** for which the polymerization

process was ended after ca. 20 s. Based on the reactivity of the 1*H*-cyclopentanaphthalene-1,3-dione-based photoinitiators, the crucial importance of carefully selecting the right acceptor has been clearly evidenced in this series of 21 dyes, since only 5 of them were remarkable photoinitiators. It also demonstrates the extensive work that has still to be done in order to combine the right donor and right electron acceptor to produce highly efficient photoinitiators. Therefore, to briefly conclude, the appealing properties of dye 5 are the followings: (1) synthesis in high reaction yield, using a Green synthesis and an easy workup, easiness of synthesis, (2) good solubility in monomers, (3) high molar extinction coefficient (dye **5** is the third most absorbing dye of the series, positioning this dye in the top 5), (4) low oxidation potential (except dyes **9**, **10**, **19** and **20** which possess a butadienyl spacer, dye 5 exhibits the lowest oxidation potential) and (5) unique bleaching properties since only this dye is capable to bleach during the polymerization process.

3. Discussion

To discuss the structure–reactivity–efficiency relationships of the dyes in these systems, the chemical mechanisms involved in the polymerization process were studied.

3.1. Proposed Chemical Mechanisms

For the photopolymerization process initiated with the three-component PIS, the chemical mechanisms can be divided into two parts: (1) dyes acting as electron donors with Iod; (2) amine (EDB) acting as the electron donor and the dyes as the electron acceptors.

3.1.1. UV-Visible Absorption and Steady State Photolysis of the Selected Ten Dyes

In this part, the ten best dyes reported in the Table 1 were selected for the steady state photolysis experiments. Their molar extinction coefficients were determined by UV-visible absorption spectroscopy and the results are summarized in the Table 2. These dyes exhibit excellent visible light absorption properties that can ensure their use in PISs upon visible LED light irradiation. For a better understanding of these absorptions, dyes 5 and 17 were selected for molecular modeling. The frontier orbitals involved in the lowest energy transition are depicted in the Figure 2. A charge transfer transition is found between the highest occupied molecular orbital (HOMO) and the lowest unoccupied molecular orbital (LUMO) localized on the electron donor (amine) or electron acceptor (indane-1,3-dione) moieties, respectively.

Table 2. Light absorption properties of the selected dyes in acetonitrile: maximum absorption wavelengths λ_{max}; molar extinction coefficients at λ_{max} (ε_{max}) and molar extinction coefficients at the emission wavelength of the LED@405 nm ($\varepsilon_{@405nm}$).

Dyes	λ_{max} (nm)	ε_{max} (M^{-1} cm^{-1})	$\varepsilon_{@405nm}$ (M^{-1} cm^{-1})
Dye **5**	498	19,900	6510
Dye **9**	526	51,110	350
Dye **10**	559	41,820	5520
Dye **14**	449	23,180	10,930
Dye **15**	504	56,620	3130
Dye **16**	498	33,740	6790
Dye **17**	522	106,650	2180
Dye **19**	564	55,720	3790
Dye **20**	598	56,280	1810
Dye **21**	696	56,330	7210

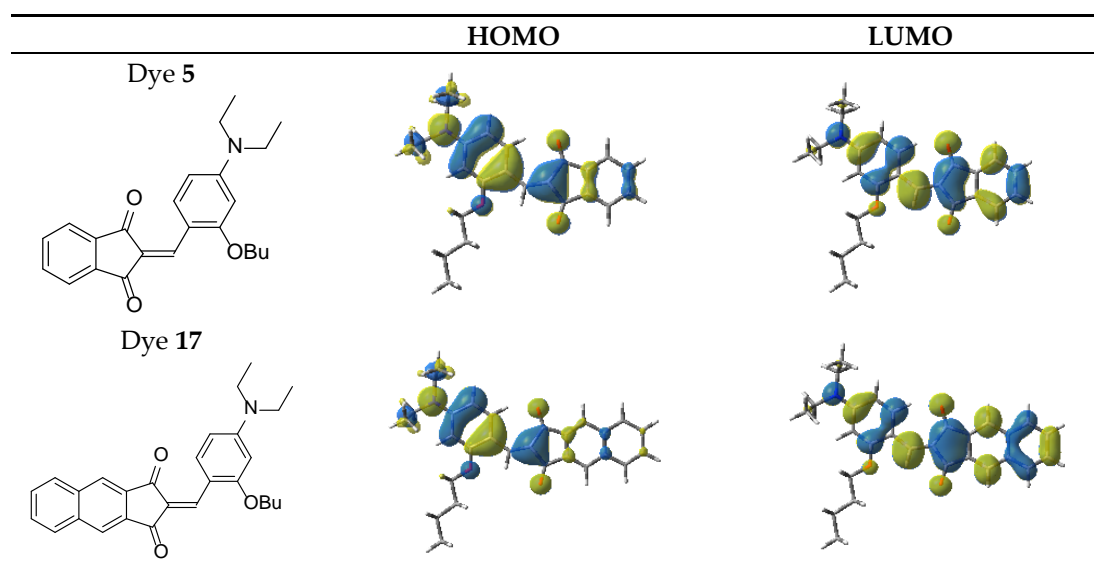|	HOMO	LUMO
Dye **5**		
Dye **17**		

Figure 2. Contour plots of HOMOs and LUMOs for dye **5** and dye **17** (isovalue = 0.02).

Photolysis of the ten best dyes shown in the Table 1, in the presence of the iodonium salt and the amine were characterized by UV-visible spectroscopy. As previously mentioned, a high molar extinction coefficient and a low oxidation potential are not sufficient for a dye to ensure the initiation of a fast polymerization process. The yield of reaction between the dye and the additives governs the reactivity as it determines at which speed the radicals will be formed. Therefore, photolysis experiments are primordial to determine the kinetic of interaction.

As evidenced by the UV-visible absorption spectra depicted in Figure 3, obvious photolysis and significant absorption decreases were observed for the photoinitiating systems comprising eight dyes among the ten examined. Among them, dyes **5**, **19**, and **20** displayed a relatively rapid photolysis process of decline, which only took 5 min, 25 min, 50 min in solution, respectively. Thus, we mainly focused on discussing the photolysis of dyes **5** and **19** to investigate their chemical mechanisms. To evidence the contribution of the additional aromatic ring on the photopolymerization process, the performances of dyes **5** and **9** were compared to those of dyes **17** and **19** bearing an additional aromatic ring. In addition, there is no obvious photolysis in the case of dyes **14**, **15** and the photolysis in the photoinitiating system with dye **16** showed an increasing process as shown in Figure 3d, i.e., the formation of a colored photoproduct.

In the case of the dye **5**-based photoinitiating system, the dye **5**/Iod/amine combination exhibited a rapid photolysis which was in agreement with the good initiating ability of this system. However, the photolysis process of the dye **17**/Iod/amine system in acetonitrile under irradiation with the LED at 405 nm is very slow as displayed in Figure 3e, due to its lower extinction coefficients ($\varepsilon_{@405}$ = 2180 M^{-1} cm^{-1}; see Table 2), which could hinder the photolysis efficiency, compared to dye **5** which exhibit a higher extinction coefficient ($\varepsilon_{@405}$ = 6510 M^{-1} cm^{-1}; see Table 2). In fact, no clear contribution of the additional aromatic ring on the photolysis process of dye **17** was evidenced.

The absorption peak of dye **19** (observed between 400 < λ < 650 nm) disappears within 25 min while the very high photostability of the dye **9**/Iod/amine combination can be clearly demonstrated. Indeed, the photolysis experiment took more time, approaching 150 min for this system. Thus, it is in accordance with the fact that a higher molar extinction coefficient is found at the emission wavelength of the LED at 405 nm for dye 19 compared to dye **9** ($\varepsilon_{@405}$ = 350 M^{-1} cm^{-1}; $\varepsilon_{@405}$ = 3790 M^{-1} cm^{-1} for dyes **9** and **19**, respectively, see Table 2). Interestingly, this trend is the opposite to that found for dyes **5**, **17**, for which the additional aromatic ring in dye **17** was considered to provide a lower extinction coefficient at the emission wavelength of the LED at 405 nm. Thus, there is no clear evidence that the additional aromatic ring governs the molar extinction coefficient or the polymerization performance in

FRP. In fact, the main factor governing the absorption at 405 nm is definitely the electron-releasing ability of the electron donor used for the design of the push–pull dyes, the electron acceptor being maintained constant in the two series.
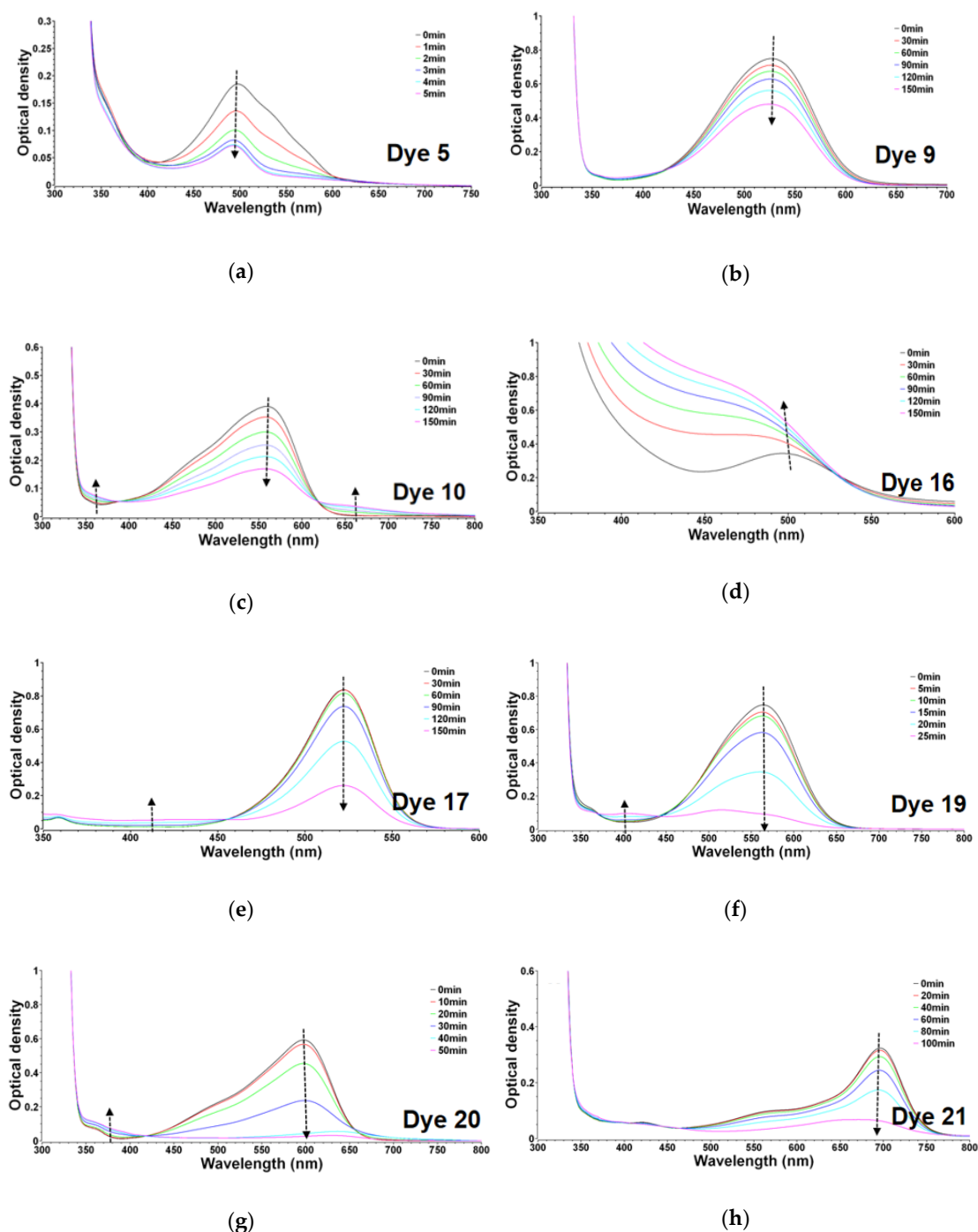

Figure 3. UV-visible absorption spectra of different dyes with co-initiators: iodonium salt (Speedcure 938, 1.46×10^{-4} M) and amine (Speedcure EDB, 4.07×10^{-4} M) upon exposure to LED@405nm under air in acetonitrile: (**a**) dye **5** (1.04×10^{-5} M), (**b**) dye **9** (1.30×10^{-5} M), (**c**) dye **10** (9.31×10^{-6} M), (**d**) dye **16** (6.46×10^{-6} M), (**e**) dye **17** (9.20×10^{-6} M), (**f**) dye **19** (1.11×10^{-5} M), (**g**) dye **20** (8.33×10^{-6} M), (**h**) dye **21** (7.56×10^{-6} M).

Compared to the performances of dye **9**, dye **10** exhibited a similar photolysis process to that observed for dye **9** in the presence of the iodonium salt and the amine, resulting from their similarity

in structures. Their respective performances in photopolymerization can be found in supplementary information. Moreover, dyes **20** and **21** showed a similar photolysis process to that observed for dye **19** even though dye **20** possesses a lower extinction coefficient at 405 nm ($\varepsilon_{@405}$ = 1810 M^{-1} cm^{-1}; see Table 2). Thus, we neglect the discussions on the photolyzes of dyes **20**, **21** as well.

To investigate the chemical mechanisms of dye-based three-component PIS, two reactions can take place: the photo-oxidation of the dye in combination with the iodonium salt or its photoreduction by the amine. Therefore, these two latter processes were separately studied. In this part, dyes **5**, **17** were selected as representative dyes, and the photolysis process of the dye/Iod and the dye/amine systems are depicted in the Figure 4. As shown in the UV-visible absorption spectra shown in Figure 4a,b presented below, dye **5** exhibited a high reactivity in two-component photoinitiating systems (dye**5**/Iod and dye **5**/EDB) which was in agreement with the high initiating ability of the dye **5**/Iod/EDB three component PISs, i.e., both photo-oxidation and photoreduction processes are probably important for dye **5**.
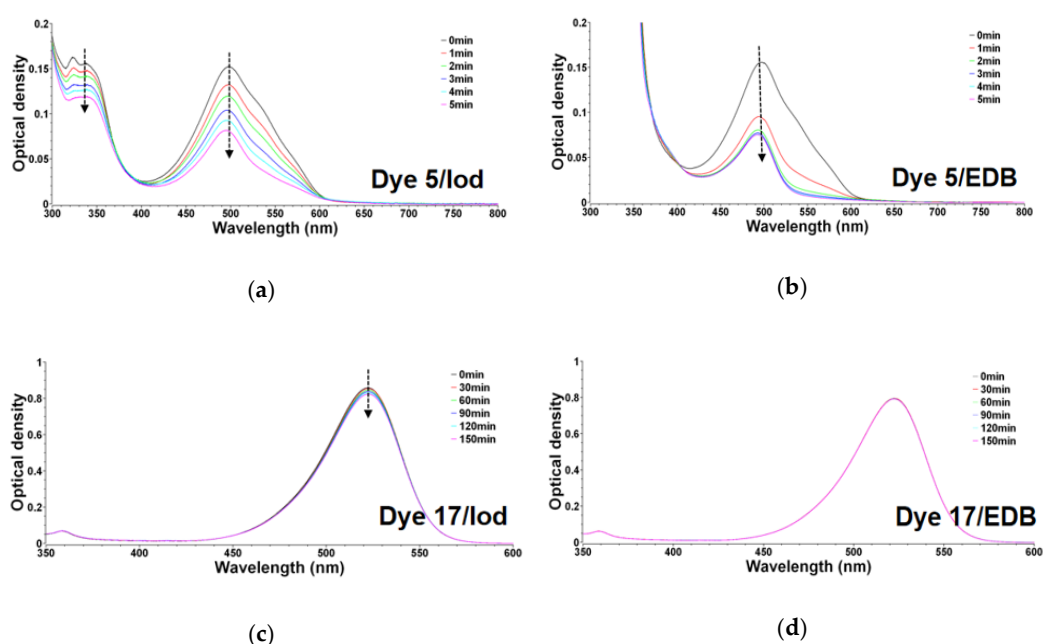

(**a**)　　　　　　　　　　　　　　　　　　　　　(**b**)

(**c**)　　　　　　　　　　　　　　　　　　　　　(**d**)

Figure 4. UV-visible absorption spectra of dyes **5**, **17** (1.04×10^{-5} M; 9.20×10^{-6} M, respectively.) (left) in the presence of the iodonium salt (Speedcure 938, 1.46×10^{-4} M) upon exposure to LED@405nm under air in the solvent of acetonitrile: (**a**) dye **5**, (**c**) dye **17** and (right) in the presence of the amine (Speedcure EDB, 4.07×10^{-4} M) upon exposure to LED@405nm under air in the solvent of acetonitrile: (**c**) dye **5**, (**d**) dye **17**.

In the presence of dye/amine interactions, no photolysis can be observed for dye **17** (characterized by a significant absorption between 400 and 600 nm in Figure 4d) in any case, for dye **17**/Iod combination, a slow photolysis is observed as shown in Figure 4c. This phenomenon can hardly be explained by clear and obvious photolysis experiments done on the dye **17**/Iod/EDB three-component PIS. The main difference between dyes **5** and **17** can probably be ascribed to their different interaction behaviors with the iodonium salt and the amine. Therefore, such speculation can be verified by investigating their chemical mechanisms, which can be carried out by ESR-spin trapping experiments. On the other hand, the photolysis process of dye **9**/Iod or dye **9**/amine in acetonitrile under irradiation of the 405nm LED is rather slow, as displayed in Figure 5a,b. For the dye **19**/EDB combination, a clear photolysis can be found as shown in Figure 5d. Therefore, the dye **19**/EDB based PIS exhibits a higher photosensitivity than the dye **9**/EDB system. For the interaction with Iod, a rather similar reactivity is found for dye **9** and dye **19**, as can be seen when comparing Figure 5a,c.
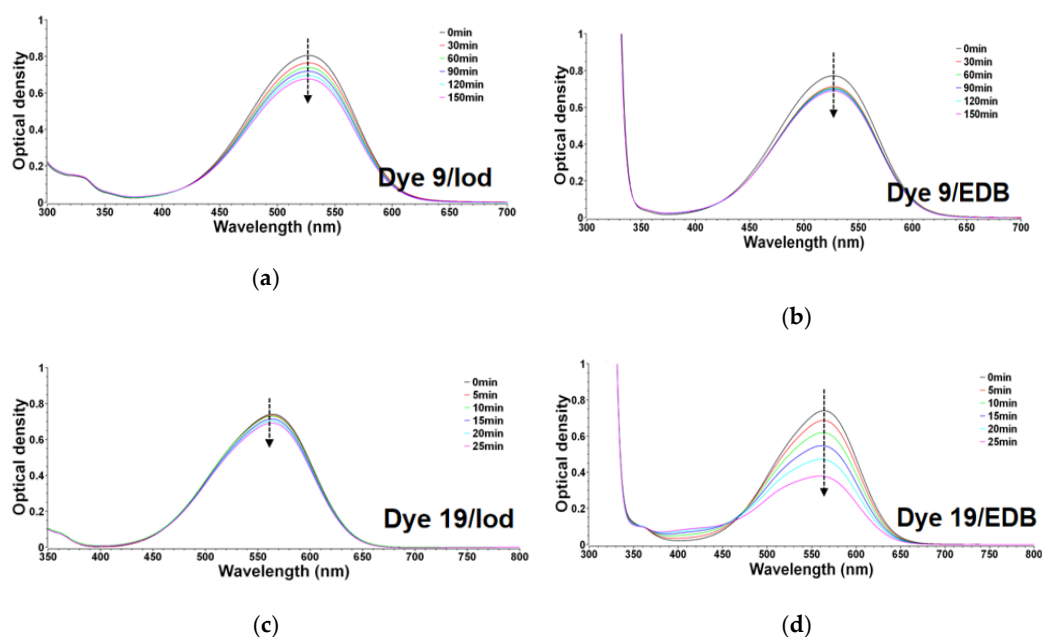
Figure 5. UV-visible absorption spectra of dyes **9**, **19** (1.30×10^{-5} M; 1.11×10^{-5} M, respectively.) (left) in the presence of iodonium salt (Speedcure 938, 1.46×10^{-4} M) upon exposure to LED@405nm under air in the solvent of acetonitrile: (**a**) dye **9**, (**c**) dye **19** and (right) in the presence of amine (Speedcure EDB, 4.07×10^{-4} M) upon exposure to LED@405nm under air in the solvent of acetonitrile: (**c**) dye **9**, (**d**) dye **19**.
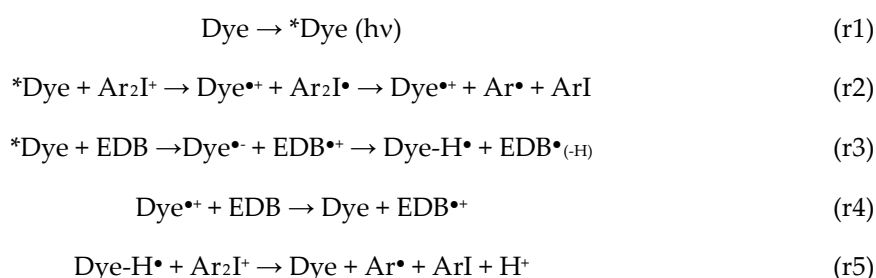
To sum up the photolysis experiments and with regards to the different experiments that have been done in this section, it can be easily seen from Figure 4a that the decoloration of the solutions of dye **5**/Iod and dye **5**/EDB can be observed within 5 min, contrarily to 150 min for dye **17**/EDB and dye **17**/Iod. Therefore a 30-fold reduction of the photolysis time is observed for dye **5**, which is gigantesque. In terms of reactivity, no comparisons are possible between the two dyes (**5** and **17**) due to the dramatic difference of production of radicals. From these results, even polymerization tests were useless in the two-component system, since it could already be anticipated that dye **5** could initiate a faster polymerization than dye **17**. The polymerization tests confirm the results obtained during photolysis experiments. However, the polymerization tests have also demonstrated the limitation of the two-component system since final monomer conversions not exceeding 40% were determined. In contrast, the three-components systems could provide the best dyes' final monomer conversions higher than 90%. Considering that a two-fold enhancement of the monomer conversions could be obtained with a few dyes, photolysis experiments were carried out with the three-component systems to get a deeper insight into the mechanism, which is developed in the next paragraph.

3.1.2. Consumption of Dyes in Photolysis Reactions

The consumption of dyes **5**, **9**, **17**, **19** in percentage vs. irradiation time is illustrated in Figure 6. In details, the consumption of dye in percentage is calculated from changes of photolysis process in the UV-visible absorption spectra. Particularly, chemical mechanisms can also be investigated by comparing the three-component PISs (dye/Iod/amine) with the two-component PIS ones (dye/Iod or dye/amine). Interestingly, it is obvious that the percentages of consumption profiles for all dyes (dye **5**, **9**, **17**, **19**) achieved by the three-component PIS (dye/Iod/amine) are higher than that reached when using the two-component PISs (dye/Iod or dye/amine), e.g., consumption of dye **5** = ~60% for dye **5**/Iod/amine vs. ~50% for dye **5**/Iod or ~30% for dye **5**/amine, as shown in Figure 6a. A faster consumption of dye **5** is also observed with the three-component system compared to the two-component system, the consumption being ended after 4 min contrarily to 5 min for the two-component system. Therefore, it

can be concluded that the higher monomer conversions obtained with the three-component system can be confidently assigned to a faster consumption of dye **5**, corresponding a faster production of radicals. With more radicals being produced simultaneously, a higher monomer conversion can be achieved.

Thus, we propose a plausible mechanism to support the formation of radicals according to the reactions depicted in the Scheme 3: r1, r2 and r3 are supposed to occur in the dye-based three-component PISs. As the generated radicals shown in Scheme 3, dye$^{\bullet+}$ radical is proposed to be generated by electron transfer from *dye to iodonium salt (r2) upon irradiation @405 nm, while dye-H$^{\bullet}$ can be formed from *dye in the presence of EDB (r3). The consumption of dyes is accelerated by the simultaneity of r2 and r3 in three-component systems. Additionally, as shown in other systems, dye$^{\bullet+}$ can react with EDB (r4) or dye-H$^{\bullet}$ with Iod (r5). Similarly, the dye **9**/Iod/amine combination seems to follow the same chemical mechanism to the dye **5**/Iod/amine PIS. Indeed, the consumption changes for all PISs comprising dye **9** (dye **9**/Iod/amine, dye **9**/Iod, or dye **9**/amine) were quite similar to that observed for the dye **5**/Iod/amine combinations, as shown in Figure 6a,b.

$$\text{Dye} \rightarrow \text{*Dye (h}\nu\text{)} \tag{r1}$$

$$\text{*Dye} + \text{Ar}_2\text{I}^+ \rightarrow \text{Dye}^{\bullet+} + \text{Ar}_2\text{I}^{\bullet} \rightarrow \text{Dye}^{\bullet+} + \text{Ar}^{\bullet} + \text{ArI} \tag{r2}$$

$$\text{*Dye} + \text{EDB} \rightarrow \text{Dye}^{\bullet-} + \text{EDB}^{\bullet+} \rightarrow \text{Dye-H}^{\bullet} + \text{EDB}^{\bullet}_{(-H)} \tag{r3}$$

$$\text{Dye}^{\bullet+} + \text{EDB} \rightarrow \text{Dye} + \text{EDB}^{\bullet+} \tag{r4}$$

$$\text{Dye-H}^{\bullet} + \text{Ar}_2\text{I}^+ \rightarrow \text{Dye} + \text{Ar}^{\bullet} + \text{ArI} + \text{H}^+ \tag{r5}$$

Scheme 3. Proposed photoinitiation step mechanisms of dyes/Iodonium/amine redox combinations.

However, despite the mechanism mentioned above, there is a dissimilar process observed in the case of the dye **19**-based PIS. Compared to the dye **9**/amine system, a slower consumption of dye **19** in the dye/Iod two-component PIS was observed during the same irradiation time, e.g., the consumption of dye **19** = ~7.3% for the dye **19**/Iod PIS vs. ~50% for the dye **9**/amine PIS, as shown in Figure 6b,d. Therefore, for dye **19**, r3 is probably favored over r2.

Interestingly, as shown in the Figure 6c, for the same irradiation time, the dye **17**/Iod/amine system led to a high consumption of the dye (~72%), whereas no obvious consumption of the dye in dye **17**/Iod or dye **17**/amine can be observed. The chemical mechanism will be discussed in the part concerning the ESR spin-trapping experiments.
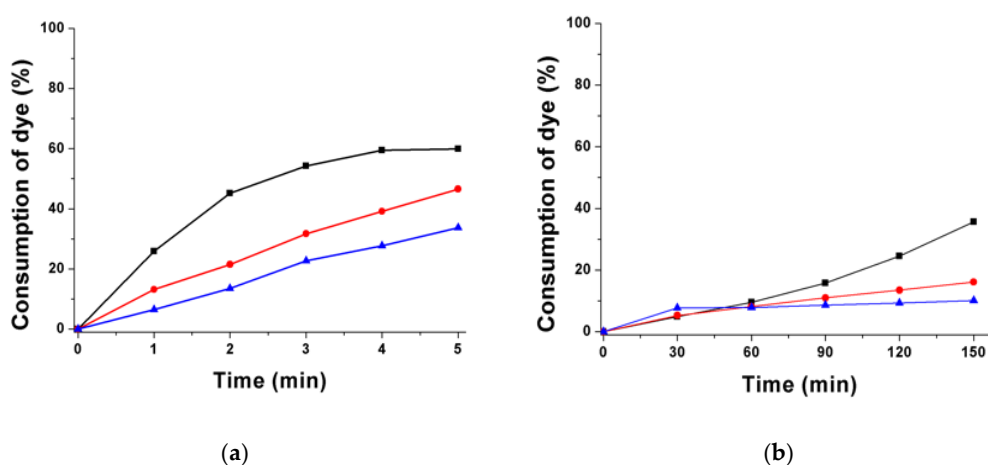

(**a**)　　　　　　　　　　　　　　　　　　　　　(**b**)

Figure 6. *Cont.*
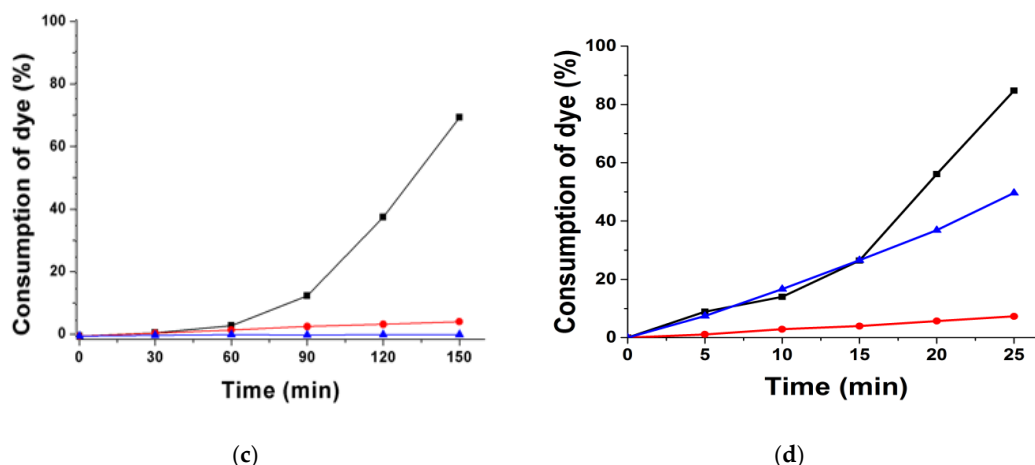
(**c**)   (**d**)

Figure 6. Consumption of dyes vs. irradiation time upon irradiation with a LED@405 nm (**a**) dye 5/Iod/amine(■); dye 5/Iod(●); dye 5/amine(▲). (**b**) dye 9/Iod/amine(■); dye 9/Iod(●); dye 9/amine(▲). (**c**) dye 17/Iod/amine(■); dye 17/Iod(●); dye 17/amine(▲). (**d**) dye 19/Iod/amine(■); dye 19/Iod(●); dye 19/amine(▲).

On the basis of the proposed mechanism depicted in the Scheme 3, the dye is partly regenerated during (r4) and (r5), enabling to introduce the dyes in catalytic amount (see the reductive cycle in Figure 7). In fact, the existence of reactions occurring in equations r2 and r3 is well established by ESR spin trapping, fluorescence quenching and ΔG experiments. These two routes certainly predominate as the consumption of the dye is a key factor governing the reactivity (see dye **5** photolysis). Concerning r4 and r5, these two additional routes can be proposed as participating in a lesser extent to the polymerization process, without clear proof of their existence.
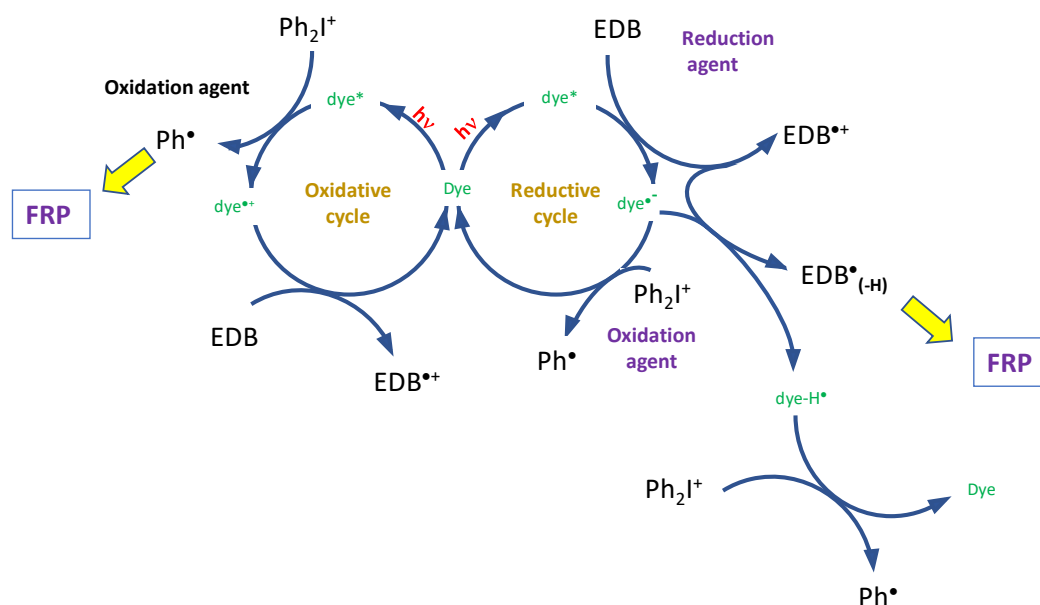
Figure 7. Mechanism involved in the generation of radicals.

Especially, compared to benchmark photoinitiators such as phenylbis(2,4,6-trimethylbenzoyl)-phosphine oxide (BAPO), camphorquinone or isopropylthioxanthone (ITX) for which percentages of 0.5–1 wt % are needed in order the polymerization process to be initiated [69,70] in the present case, an amount as low as 0.1 wt % could be used while maintaining exceptional final monomer conversions

such as with the dyes **5**, **14**, **16**, **17**, **19** and **20**, for which final monomer conversions higher than 90% could be obtained within 10–20 s.

3.1.3. Chemical Mechanisms in Electron Transfer Reactions for Dyes

The theoretical feasibility of the interactions between dye/Iod (or dye/amine) was investigated by calculations of the free energy changes (ΔG_{Iod} or ΔG_{EDB}, respectively) for the electron transfer reactions. According to the equations (Equation (1) or Equation (2)), ΔG_{Iod} or ΔG_{EDB} were determined from the oxidation potential E_{ox} (or from the reduction potential or E_{red}, respectively) and the first singlet excited state energy (E_{S1}). The oxidation potentials (or reduction potentials) of dyes **5**, **9**, **17**, **19** have been reported by literature [43] and their first singlet excited state energies (E_{S1}) can be calculated from the crossing point of the UV-visible absorption and the fluorescence spectra, as shown in Figure 8. The results are gathered in the Table 3.

Fluorescence quenching experiments were carried out to evaluate the efficiency of the dye/Iod interaction. Interestingly, Iod was determined as acting as a relatively good quencher for dyes **5** and 16, as displayed in Figure 9 and Figure S2, respectively. As shown in the Stern–Volmer treatment data, a linear quenching for dye **5** was found, whereas there was only a weak decrease for dyes **9** and **19**. The Stern–Volmer constants (Ksv) and the electron transfer quantum yields ($\phi_{et\,(S1)}$) for dyes **5**, **9**, **16** and **19** with Iod were also calculated, as shown in Table 3. Moreover, obvious fluorescence quenching was not for both the dye **17**/Iod and the dyes/amine combinations.
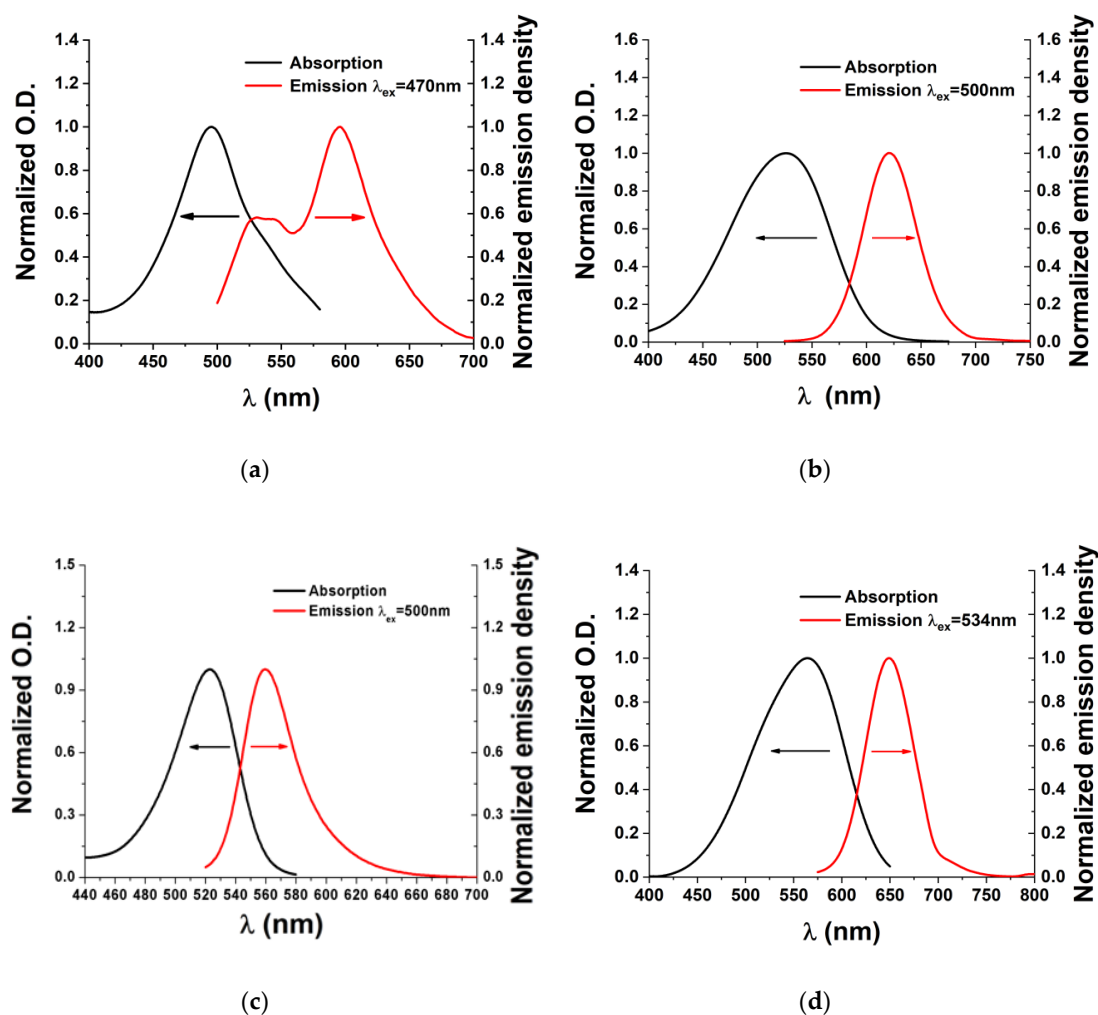

Figure 8. Singlet state energy determination in acetonitrile for: (**a**) dye **5**; (**b**) dye **9**; (**c**): dye **17**; (**d**) dye **19**.

Table 3. Parameters characterizing the chemical mechanisms associated with dyes **5, 9, 16, 17, 19** in acetonitrile [a].

	Dye 5	**Dye 9**	**Dye 16**	**Dye 17**	**Dye 19**
E_{ox} (eV)	0.54	0.49	0.79	0.79	0.49
E_{red} (eV)	−1.30	−1.30	−1.31	−1.31	−1.22
E_{S1} (eV) [b]	2.32	2.0_2	2.29	2.29	2.12
E_{T1} (eV) [c]	2.1	1.6	1.9	2.0	1.6
ΔG^{S1}_{Iod} (eV)	−1.08	−0.83	−0.80	−0.80	−0.93
ΔG^{S1}_{EDB} (eV)	−0.02	0.29	0.02	0.02	0.10
ΔGet^{T1}_{Iod} (eV)	−0.86	−0.41	−0.41	−0.51	−0.41
ΔGet^{T1}_{EDB} (eV)	0.21	0.7	0.41	0.31	0.62
K^{sv}_{Iod} (M^{-1})	359	2.62	64	-	1.86
$\phi^{et(S1)}_{Iod}$ [d]	0.939	0.101	0.732	-	0.074

[a] A re-evaluated value of reduction potential of −0.7 V is used according to ref. [71]; [b] From the values presented in ref. [43]; [c] Calculated triplet state energy level at DFT level; [d] From the equation presented in ref. [45].

(**a**)

(**b**)
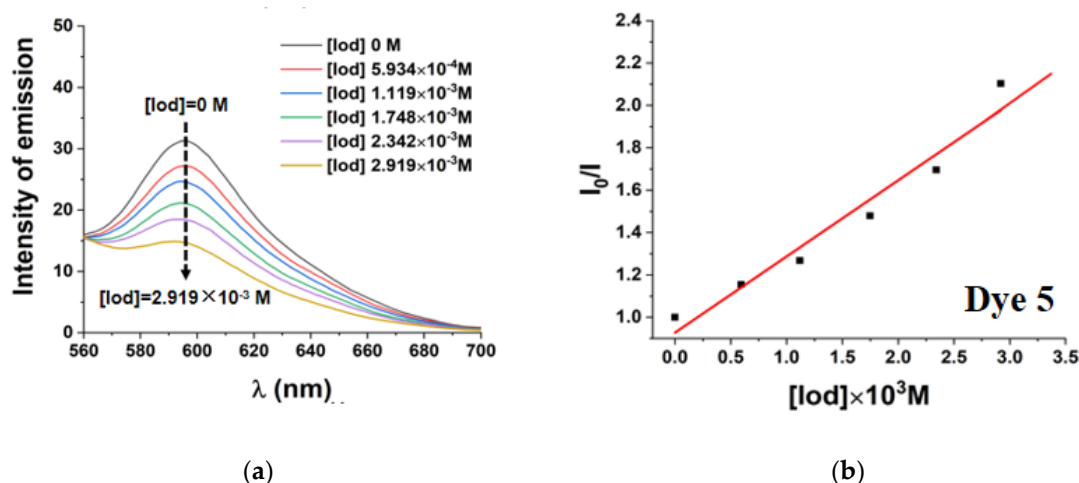
Figure 9. (**a**) Fluorescence quenching of dye **5** by iodonium salts; (**b**) Stern–Volmer treatment for the dye **5**/Iodonium salts fluorescence quenching.

The calculated triplet state energies (density functional theory level) for a series of representative dyes are gathered in the Table 3. A triplet state pathway cannot be ruled out for dye/Iod interaction ($\Delta G < 0$; Table 3). In contrast, such a triplet state interaction is not favorable for the dye/amine combination ($\Delta G > 0$; Table 3).

3.1.4. ESR Spin-Trapping Experiments

For a better understanding of the dye/Iod/amine interaction, ESR-spin trapping experiments were carried out on dye **5**/Iod/amine (or dye **17**/Iod/amine) and dye **5**/Iod solution under N_2 in presence of PBN as the spin trap agent (Figure 10 for dye **5**, see Figure S3 for dye **17** in the supplementary materials). The simulation gave the following hyperfine coupling constants (hfc) constants for the PBN spin adducts: $a_N = 14.4$ G; $a_H = 2.1$ G for the dye 5/Iod PISs ($a_N = 14.7$ G; $a_H = 2.8$ G for the dye **17**/Iod/amine PISs) which suggests the generation of the radical $(CH_3)_3C_6H_4\bullet$ fully matching to literature data [72]. It also suggests that the redox reaction (r2) between dye **5** and Iod takes place where Iod acts as an oxidizing agent leading to the formation of aryl radicals.
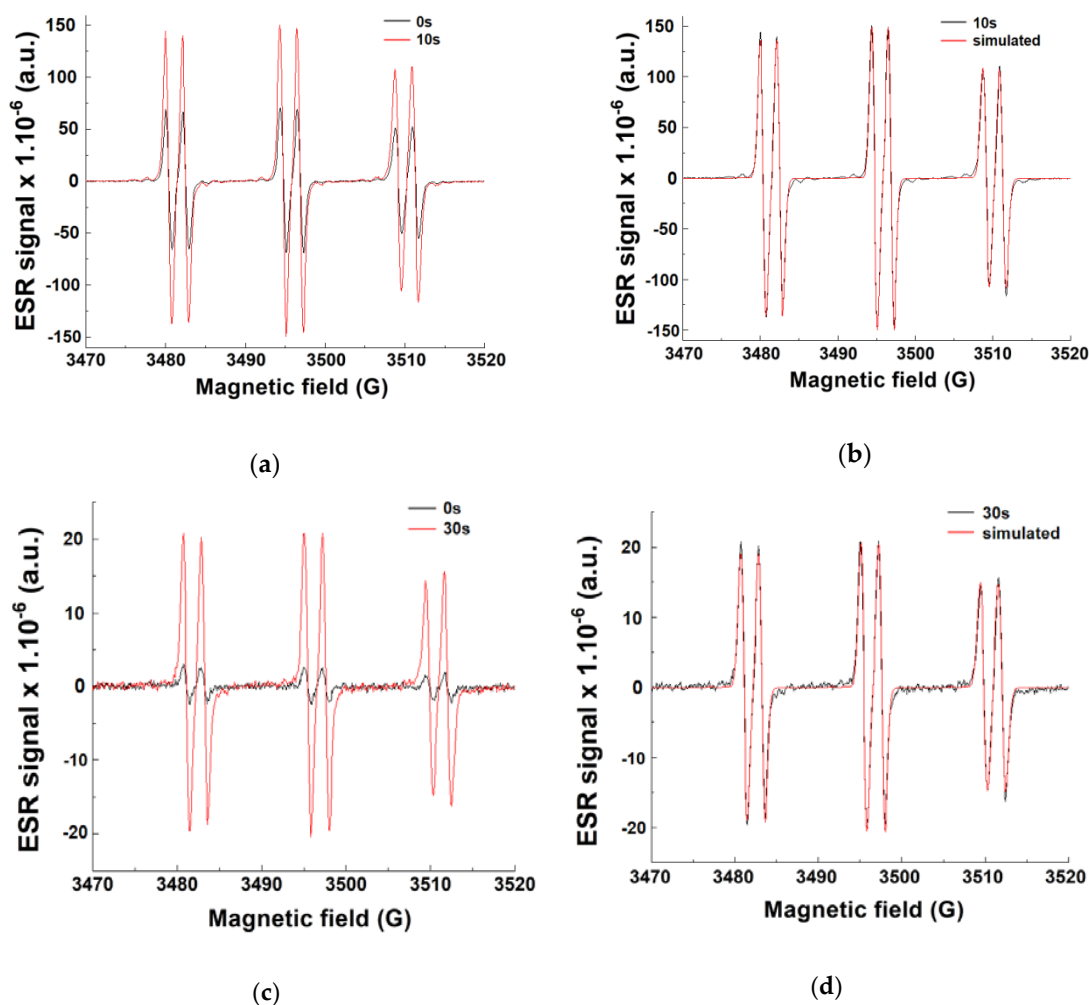
Figure 10. Electron spin resonance (ESR) spectra obtained from ESR-spin trapping experiment using PBN = 2 mg/mL (as spin trap agent); iodonium salt (Iod) or amine (EDB) = 12.6 mg/mL and dye **5** = 0.8 mg/mL in *tert*-butylbenzene under N_2: (**a**) dye **5**/Iod, irradiation time = 0 s (black) and = 10 s (red) spectra; (**b**) dye **5**/Iod, irradiation time =10 s (black) and simulated (red) spectra; (**c**) dye **5**/amine, irradiation time = 0 s (black) and = 30 s (red) spectra; (**d**) dye **5**/amine, irradiation time = 30 s (black) and simulated (red) spectra.

Additional ESR-spin trapping experiments carried out by irradiating the dye **5**/amine solution were carried out, and the results are presented in Figure 10c,d. Interestingly, a radical adduct corresponding to PBN/ArNCH$_3$CH$_2$• adduct is detected and characterized by a_N = 14.4 G; a_H = 2.2 G in agreement with literature data [73]. As expected, there is no radical observed for the dye 17/amine PISs. All these data are in agreement with the chemical mechanisms presented above in the Scheme 3.

3.2. Laser Write Experiments Based on Dyes **5** and **19**

Some laser writing experiments using different PISs (dye/Iod/amine) in Ebecryl 40 were performed and tridimensional patterns (TSY) were fabricated successfully, as shown in Figure 11. Dyes **5** and **19** were selected due to their good performances for the FRP of Ebecryl 40. These two dyes were selected as being the best candidates of the two series of dyes (for irradiation at 405 nm). The 3D patterns were characterized by profilometric observations using numerical optical microscopy. As expected, efficient photopolymerization processes occurred in the irradiated area, and the patterns clearly illustrated excellent 3D profiles, smooth surfaces and excellent spatial resolution, as displayed in Figure 11b,d). Laser writing experiments with the dye **17**/Iod/amine PIS were also carried out. Other experiments

were performed with the dyes **5** or **19** (see Figure S4 in the supplementary materials) but with a lower spatial resolution.
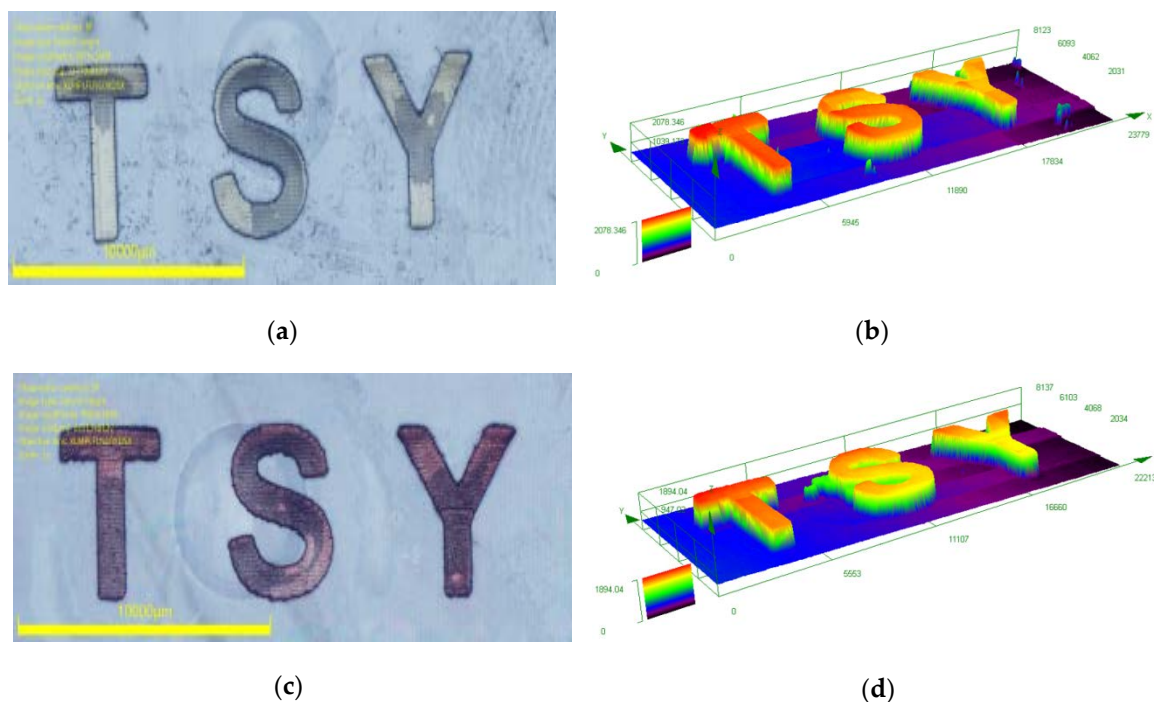

(**a**)

(**b**)

(**c**)

(**d**)

Figure 11. Free radical photopolymerization experiments for laser write experiments for different dye-based three-component photoinitiating systems in Ebecryl 40. Characterization of the 3D patterns by numerical optical microscopy: (left) top surface morphology (right) 3-D overall appearance of the 3D pattern using dye/Iod/amine (0.1%/2%/2% w/w/w) in Ebecryl 40: (**a**,**b**) for dye **5**/Iod/EDB; (**c**,**d**) for dye **19**/Iod/EDB.

4. Materials and Methods

4.1. Dyes

Dyes **1–20** used as photoinitiators were prepared with the highest purity as reported in [43]. Their corresponding molecular structures are given in the Scheme 1 and marked by their real colors.

Synthesis of 2-(2-(3,3-bis(4-(dimethylamino)phenyl)allylidene)-3-oxo-2,3-dihydro-1H-cyclopenta[b] naphthalen-1-ylidene)malononitrile (dye **21**)

2-(3-oxo-2,3-dihydro-1H-cyclopenta[b]naphthalen-1-ylidene)malononitrile (0.5 g, 2.05 mmol, M = 244.25 g/mol) and 3,3-*bis*(4-(dimethylamino)phenyl)acrylaldehyde (0.60 g, 2.05 mmol, M = 294.40 g/mol) were dissolved in absolute ethanol (50 mL) and a few drops of piperidine were added. The reaction mixture was introduced a preheated bath at 110 °C and progress of the reaction was monitored by TLC. After cooling, a precipitate formed. It was filtered off, washed several times with ethanol and dried under vacuum (0.96 g, 90% yield). ^{1}H NMR (CDCl$_3$) δ: 3.11 (s, 12H), 6.70 (d, 2H, J = 8.0 Hz), 6.79 (d, 2H, J = 7.6 Hz), 7.29 (d, 2H, J = 7.9 Hz), 7.54 (d, 2H, J = 8.0 Hz), 7.61–7.63 (m, 2H), 7.98–8.05 (m, 2H), 8.25 (s, 1H), 8.44 (d, 1H, J = 12.6 Hz), 8.78 (d, 1H, J = 12.6 Hz), 9.05 (s, 1H); ^{13}C NMR (CDCl$_3$) δ: 40.1, 63.4, 111.5, 111.7, 115.8, 116.8, 121.1, 123.2, 123.7, 128.7, 128.9, 129.9, 130.4, 133.8, 134.0, 134.4, 135.1, 135.2, 136.0, 147.9, 152.7, 153.0, 160.9, 169.9, 189.6; Anal. Calc. for C$_{35}$H$_{28}$N$_4$O: C, 80.7; H, 5.4; O, 3.1; Found: C, 80.8; H, 5.6; O, 3.2; HRMS (ESI MS) m/z: theor: 521.2336 found: 521.2335 [M + H]$^+$ detected).

4.2. Other Materials

The photopolymerizable monomer (Ebecryl 40) was obtained from Allnex (Bruxelles, Belgium). The other chemicals, e.g., iodonium salt (Speedcure 938) and the amine (ethyl dimethylaminobenzoate (EDB; also noted Speedcure EDB) were obtained from Lambson Ltd. (Wetherby, UK), and their corresponding chemical structures are depicted in the Scheme 2. Particularly, to highlight the potential applications in Green chemistry, polymerization experiments were carried out in solvent-free conditions in mild conditions.

4.3. Free Radical Polymerization (FRP) Process Monitored by Real Time Fourier Transformed Infrared Spectroscopy (RT-FTIR)

The different three-component systems were prepared with a dye/iodonium salts (Iod also noted Speedcure 938) /ethyl dimethylaminobenzoate (amine = EDB, also noted Speedcure EDB) combination and exposed to a LED emitting at 405 nm (I_0 = 110 mW cm^{-2}) under air, at room temperature, and all samples were dropped between two polypropylene films with two drops of resin deposited in laminate for the FRP. Moreover, their weight contents were calculated from the monomer (Ebecryl 40) content and kept at 0.1%/2%/2% (w/w/w), respectively.

To monitor the FRP process, the conversion of the C=C double bond of the monomer was continuously followed by real time FTIR spectroscopy (JASCO FTIR 4100) and focused on the stretching vibration peak of acrylate C=C double bond at ~1630 cm^{-1} versus irradiation time [74–76].

4.4. UV-Visible Absorption, Photolysis and Fluorescent Properties

The UV-Visible absorption properties and the steady state photolysis experiments of the three-component PISs were studied by JASCO V730 UV-visible spectrometer (Tokyo Japan). The fluorescence properties were studied using a JASCO FP-6200 spectrofluorimeter (Tokyo, Japan).

4.5. Redox Potentials

The redox potentials for dye **5**, **9**, **16**, **17**, **19** (oxidation potential E_{ox} and reduction potential E_{red}) were determined in acetonitrile while using tetrabutylammonium hexafluorophosphate as the supporting electrolyte (potential vs. saturated calomel electrode, SCE), the procedure was reported in [43]. Furthermore, the free energy change of singlet state ΔG^{S1}_{Iod} or ΔG^{S1}_{EDB} for electron transfer reaction was calculated from Equation (1) or Equation (2) [77] determined by E_{ox}, E_{red}, and $E^*(Es_1)$. Here, E_{ox}, E_{red}, and $E^*(Es_1)$ are the oxidation potential of the electron donor (EDB), the reduction potential of the electron acceptor (Iod), the excited state energy level (calculated from the crossing point of UV-visible and fluorescence spectra), respectively. Similarly, the free energy change of triplet state ΔG_{et} was calculated from Equations 3 and 4 [42] where the triplet state energy level is noted $E^*(E_{T1})$. Particularly, $E^*(E_{T1})$ was extracted from molecular energy level calculations (Gaussian 03 suite of programs). The reduction potential of iodonium was −0.7V and the oxidation potential of EDB was 1.0V according to literature data [45,71].

$$\Delta G^{S1}_{Iod} = E_{ox} - (-0.7) - E^* (E_{S1}) \tag{1}$$

$$\Delta G^{S1}_{EDB} = 1 - (E_{red}) - E^* (E_{S1}) \tag{2}$$

$$\Delta G^{et}_{Iod} = E_{ox} - (-0.7) - E^* (E_{T1}) \tag{3}$$

$$\Delta G^{et}_{EDB} = 1 - (E_{red}) - E^* (E_{T1}) \tag{4}$$

4.6. 3D Printing Experiments

The photosensitive formulations (Ebecryl 40, PISs included) was deposited onto a homemade tank (2mm thickness) and polymerized under air by 3D printing to produce specific tridimensional patterns upon spatially controlled irradiation by a laser diode @405 nm with spot size around 50 μm.

The printed 3D patterns were characterized through a numerical optical microscope (DSX-HRSU, OLYMPUS corporation, Tokyo Japan) [78,79].

4.7. Electron Spin Resonance (ESR) Spin Trapping (ESR-ST)

Electron spin resonance-spin trapping experiments were carried out using an X-band spectrometer (Bruker EMXplus, Karlruhe Germany). The radicals were observed under a nitrogen saturated atmosphere at room temperature. *N-tert*-Butyl-phenylnitrone (PBN) was used as a spin trap agent in *tert*-butylbenzene [75,76]. ESR spectra simulations were carried out using PEST WINSIM software.

4.8. Computational Procedure

Geometry optimizations were carried out at the UB3LYP/6-31G* level. Geometries were frequency checked. The molecular orbitals (MOs) involved in these transitions were extracted [80,81].

5. Conclusions

In this research, a series of 21 new dyes was used for the elaboration of new photoinitiating systems capable of initiating high performance photopolymerization. Specifically, two series of indane-1,3-dione and 1*H*-cyclopentanaphthalene-1,3-dione derivatives appeared as being efficient photoinitiators for 405 nm LED light induced photopolymerization accompanied with an iodonium salt and an amine. The results on polymerization kinetics of monomer (Ebecryl 40) in the presence of new dye-contained photoinitiating systems were systematically investigated and dye **5** and **17** were evaluated as reliable photoinitiators. Moreover, the steady state photolysis of dye-based photoinitiating systems was found and their proposed chemical mechanisms have been discussed by consumption profiles of dyes. The electron transfer between dyes, iodonium salt and amine in the FRP process are confirmed by both free energy change calculations and ESR experiments. Interestingly, very good photobleaching properties and fluorescence quenching of dye **5** were detected.

It was also found that both good light absorption properties and excellent photochemical reactivity in the excited state processes (redox reactions) are required for the dyes to reach efficient photoinitiating systems.

Finally, some 3D patterns were written using these three-component photoinitiating systems. To conclude, our research contributes to improve the knowledge of photopolymerization carried out at 405 nm with LEDs by the development of new PISs comprising push–pull chromophores. By improving the electron accepting ability of the naphthalene-based electron acceptor, PISs operating in the near infrared region could be developed and the synthesis of such dyes is currently under progress.

References

1. Ganster, B.; Fischer, U.K.; Moszner, N.; Liska, R. New photocleavable structures. Diacylgermane-based photoinitiators for visible light curing. *Macromolecules* **2008**, *41*, 2394–2400. [CrossRef]

2. Ganster, B.; Fischer, U.K.; Moszner, N.; Liska, R. New Photocleavable Structures, 4: Acylgermane-Based Photoinitiator for Visible Light Curing. *Macromol. Rapid Commun.* **2008**, *29*, 57–62. [CrossRef]

3. Cook, W.D.; Chen, F. Enhanced visible radiation photopolymerization of dimethacrylates with the three component thioxanthone (CPTXO)–amine–iodonium salt system. *Polym. Chem.* **2015**, *6*, 1325–1338. [CrossRef]

4. Xiao, P.; Wang, Y.; Dai, M.; Wu, G.; Shi, S.; Nie, J. Synthesis and photopolymerization kinetics of benzophenone piperazine one-component initiator. *Polym. Adv. Technol.* **2008**, *19*, 409–413. [CrossRef]

5. Karaca, N.; Balta, D.K.; Ocal, N.; Arsu, N.J. Mechanistic studies of thioxanthone–carbazole as a one-component type II photoinitiator. *J. Lumin.* **2014**, *146*, 424–429. [CrossRef]

6. Esen, D.S.; Temel, G.; Balta, D.K.; Allonas, X.; Arsu, N. One-component thioxanthone acetic acid derivative photoinitiator for free radical polymerization. *Photochem. Photobiol.* **2014**, *90*, 463–469. [CrossRef] [PubMed]

7. Vitale, A.; Sangermano, M.; Bongiovanni, R.; Burtscher, P.; Moszner, N. Visible light curable restorative composites for dental applications based on epoxy monomer. *Materials* **2014**, *7*, 554–562. [CrossRef] [PubMed]

8. Fors, B.P.; Hawker, C. Control of a living radical polymerization of methacrylates by light. *J. Angew. Chem. Int. Ed.* **2012**, *51*, 8850–8853. [CrossRef]

9. Konkolewicz, D.; Schrööder, K.; Buback, J.; Bernhard, S.; Matyjaszewski, K. Visible light and sunlight photoinduced ATRP with ppm of Cu catalyst. *ACS Macro Lett.* **2012**, *1*, 1219–1223. [CrossRef]

10. Haddleton, D.M. Polymer chemistry: Rooftop reactions. *Nat. Chem.* **2013**, *5*, 366–368. [CrossRef]

11. Treat, N.J.; Fors, B.P.; Kramer, J.W.; Christianson, M.; Chiu, C.-Y.; Alaniz, J.R.D.; Hawker, C.J. Controlled radical polymerization of acrylates regulated by visible light. *ACS Macro Lett.* **2014**, *3*, 580–584. [CrossRef]

12. Xu, J.; Boyer, C. Visible light photocatalytic thiol–ene reaction: An elegant approach for fast polymer post-functionalization and step-growth polymerization. *Macromolecules* **2015**, *48*, 520–529. [CrossRef]

13. Kenning, N.S.; Ficek, B.A.; Hoppe, C.C.; Scranton, A.B. Spatial and temporal evolution of the photoinitiation rate for thick polymer systems illuminated by polychromatic light: Selection of efficient photoinitiators for LED or mercury lamps. *Polym. Int.* **2008**, *57*, 1134–1140. [CrossRef]

14. Lalevée, J.; Blanchard, N.; Tehfe, M.A.; Peter, M.; Morlet-Savary, F.; Fouassier, J.P. A novel photopolymerization initiating system based on an iridium complex photocatalyst. *Macromol. Rapid Commun.* **2011**, *32*, 917–920. [CrossRef] [PubMed]

15. Lalevée, J.; Telitel, S.; Xiao, P.; Lepeltier, M.; Dumur, F.; Morlet-Savary, F.; Gigmes, D.; Fouassier, J.P. Metal and metal-free photocatalysts: Mechanistic approach and application as photoinitiators of photopolymerization. *Beilstein J. Org. Chem.* **2014**, *10*, 863–876. [CrossRef] [PubMed]

16. Lalevée, J.; Allonas, X.; Fouassier, J.P. Addition of carbon-centered radicals to double bonds: Influence of the alkene structure. *J. Org. Chem.* **2005**, *70*, 814–819. [CrossRef]

17. Geérard, V.; Ay, E.; Morlet-Savary, F.; Graff, B.; Galopin, C.; Ogren, T.; Mutilangi, W.; Lalevée, J. Thermal and photochemical stability of anthocyanins from black carrot, grape juice, and purple sweet potato in model beverages in the presence of ascorbic acid. *J. Agric. Food Chem.* **2019**, *67*, 5647–5660. [CrossRef]

18. Aparicio, J.L.; Elizalde, M. Migration of photoinitiators in food packaging: A Review. *Packag. Technol. Sci.* **2015**, *28*, 181–203. [CrossRef]

19. Lago, M.A.; Rodríguez-Bernaldo de Quirós, A.; Sendón, R.; Bustos, J.; Nieto, M.T.; Paseiro, P. Photoinitiators: A food safety review. *Food Addit. Contam. Part A* **2015**, *32*, 779–798. [CrossRef]

20. Oesterreicher, A.; Roth, M.; Hennen, D.; Mostegel, F.H.; Edler, M.; Kappaun, S.; Griesser, T. Low migration type I photoinitiators for biocompatible thiol-ene formulations. *Eur. Polym. J.* **2017**, *88*, 393–402. [CrossRef]

21. Taschner, R.; Gauss, P.; Knaack, P.; Liska, R. Biocompatible photoinitiators based on poly-α-ketoesters. *J. Polym. Sci.* **2020**, *58*, 242–253. [CrossRef]

22. Leonhardt, S.; Klare, M.; Scheer, M.; Fischer, T.; Cordes, B.; Eblenkamp, M. Biocompatibility of photopolymers for additive manufacturing. *Curr. Dir. Biomed. Eng.* **2016**, *2*, 113–116. [CrossRef]

23. Bagheri, A.; Jin, J. Photopolymerization in 3D Printing. *ACS Appl. Polym. Mater.* **2019**, *1*, 593–611. [CrossRef]

24. Fouassier, J.-P.; Ruhlmann, D.; Graff, B.; Morlet-Savary, F.; Wieder, F. Excited state processes in polymerization photoinitiators. *Progr. Org. Coat.* **1995**, *25*, 235–271. [CrossRef]

25. Bouzrati-Zerelli, M.; Guillaume, N.; Goubard, F.; Bui, T.-T.; Villotte, S.; Dietlin, C.; Morlet-Savary, F.; Gigmes, D.; Fouassier, J.-P.; Dumur, F.; et al. A novel class of photoinitiators with a thermally activated delayed fluorescence (TADF) property. *New J. Chem.* **2018**, *42*, 8261–8270. [CrossRef]

26. Zivic, N.; Bouzrati-Zerelli, M.; Kermagoret, A.; Dumur, F.; Fouassier, J.-P.; Gigmes, D.; Lalevée, J. Photocatalysts in polymerization reactions. *ChemCatChem* **2016**, *8*, 1617–1631. [CrossRef]

27. Dadashi-Silab, S.; Doran, S.; Yagci, Y. Photoinduced electron transfer reactions for macromolecular syntheses. *Chem. Rev.* **2016**, *116*, 10212–10275. [CrossRef]

28. Dadashi-Silab, S.; Aydogana, C.; Yagci, Y. Shining a light on an adaptable photoinitiator: Advances in photopolymerizations initiated by thioxanthones. *Polym. Chem.* **2015**, *6*, 6595–6615. [CrossRef]

29. Mitterbauer, M.; Knaack, P.; Naumov, S.; Markovic, M.; Ovsianikov, A.; Moszner, N.; Liska, R. Acylstannanes: Cleavable and highly reactive photoinitiators for radical photopolymerization at wavelengths above 500 nm with excellent photobleaching behavior. *Angew. Chem. Int. Ed.* **2018**, *57*, 12146–12150. [CrossRef]

30. Radebner, J.; Eibel, A.; Leypold, M.; Jungwirth, N.; Pickl, T.; Torvisco, A.; Fischer, R.; Fischer, U.K.; Moszner, N.; Gescheidt, G.; et al. Tetraacylstannanes as long-wavelength visible-light photoinitiators with intriguing low toxicity. *Chem. Eur. J.* **2018**, *24*, 8281–8285. [CrossRef]

31. Eibel, A.; Fast, D.E.; Gescheidt, G. Choosing the ideal photoinitiator for free radical photopolymerizations: Predictions based on simulations using established data. *Polym. Chem.* **2018**, *9*, 5107–5115. [CrossRef]

32. Eibel, A.; Radebner, J.; Haas, M.; Fast, D.E.; Freißmuth, H.; Stadler, E.; Faschauner, P.; Torvisco, A.; Lamparth, I.; Moszner, N.; et al. From mono-to tetraacylgermanes: Extending the scope of visible light photoinitiators. *Polym. Chem.* **2018**, *9*, 38–47. [CrossRef]

33. Bouzrati-Zerelli, M.; Zivic, N.; Dumur, F.; Gigmes, D.; Graff, B.; Fouassier, J.-P.; Lalevée, J. New violet to yellow light sensitive diketopyrrolo-pyrrole photoinitiators: High performance systems with unusual bleaching properties and solubility in water. *Polym. Chem.* **2017**, *8*, 2028–2040. [CrossRef]

34. Tehfe, M.-A.; Dumur, F.; Telitel, S.; Gigmes, D.; Contal, E.; Bertin, D.; Morlet-Savary, F.; Graff, B.; Fouassier, J.-P.; Lalevée, J. Zinc-based metal complexes as new photocatalysts in polymerization initiating systems. *Eur. Polym. J.* **2013**, *49*, 1040–1049. [CrossRef]

35. Li, J.; Hao, Y.; Zhong, M.; Tang, L.; Nie, J.; Zhu, X. Synthesis of furan derivative as LED light photoinitiator: One-pot, low usage, photobleaching for light color 3D printing. *Dyes Pigm.* **2019**, *165*, 467–473. [CrossRef]

36. Kamoun, E.A.; Winkel, A.; Eisenburger, M.; Menzel, H. Carboxylated camphorquinone as visible-light photoinitiator for biomedical application: Synthesis, characterization, and application. *Arab. J. Chem.* **2016**, *9*, 745–754. [CrossRef]

37. Zhang, J.; Zivic, N.; Dumur, F.; Xiao, P.; Graff, B.; Gigmes, D.; Fouassier, J.-P.; Lalevée, J. A benzophenone-naphthalimide derivative as versatile photoinitiator for near UV and visible lights. *J. Polym. Sci. A Polym. Chem.* **2015**, *53*, 445–451. [CrossRef]

38. Bonardi, A.H.; Dumur, F.; Grant, T.M.; Noirbent, G.; Gigmes, D.; Lessard, B.H.; Fouassier, J.-P.; Lalevée, J. High performance near infrared (NIR) photoinitiating systems operating under low light intensity and in presence of oxygen. *Macromolecules* **2018**, *51*, 1314–1324. [CrossRef]

39. Garra, P.; Dietlin, C.; Morlet-Savary, F.; Dumur, F.; Gigmes, D.; Fouassier, J.-P.; Lalevée, J. Photopolymerization processes of thick films and in shadow areas: A review for the access to composites. *Polym. Chem.* **2017**, *8*, 7088–7101. [CrossRef]

40. Guda, R.; Bhaskar, A.; Goodson, T. Ultrafast excited state relaxation dynamics of branched donor-π-acceptor chromophore: Evidence of a charge-delocalized state. *J. Phys. Chem. B* **2006**, *110*, 20872–20878.

41. Bures, F. Fundamental aspects of property tuning in push–pull molecules. *RSC Adv.* **2014**, *4*, 58826–58851. [CrossRef]

42. Pigot, C.; Noirbent, G.; Peralta, S.; Duval, S.; Nechab, M.; Gigmes, D.; Dumur, F. Unprecedented Nucleophilic Attack of Piperidine on the Electron Acceptor during the Synthesis of Push-Pull Dyes by a Knoevenagel Reaction. *Helv. Chim. Acta* **2019**, *102*, e1900229. [CrossRef]

43. Pigot, C.; Noirbent, G.; Bui, T.T.; Péralta, S.; Gigmes, D.; Nechab, M.; Dumur, F. Push-Pull Chromophores Based on the Naphthalene Scaffold: Potential Candidates for Optoelectronic Applications. *Materials* **2019**, *12*, 1342. [CrossRef] [PubMed]

44. Xiao, P.; Zhang, J.; Dumur, F.; Tehfe, M.A.; Morlet-Savary, F.; Graff, B.; Gigmes, D.; Fouassier, J.-P.; Lalevée, J. Visible light sensitive photoinitiating systems: Recent progress in cationic and radical photopolymerization reactions under soft conditions. *Prog. Polym. Sci.* **2015**, *41*, 32–66. [CrossRef]

45. Fouassier, J.-P.; Lalevée, J. *Photoinitiators for Polymer Synthesis—Scope, Reactivity, and Efficiency*; John Wiley & Sons: Weinheim, Germany, 2012.

46. Tehfe, M.A.; Lalevée, J.; Morlet-Savary, F.; Graff, B.; Blanchard, N.; Fouassier, J.P. Organic photocatalyst for polymerization reactions: 9,10-*bis*[(triisopropylsilyl)ethynyl]anthracene. *ACS Macro Lett.* **2012**, *1*, 198–203. [CrossRef]

47. Oster, G. Dye-Sensitized Photopolymerization. *Nature* **1954**, *173*, 300–301. [CrossRef]

48. Tehfe, M.-A.; Dumur, F.; Graff, B.; Gigmes, D.; Fouassier, J.-P.; Lalevée, J. Blue-to-red light sensitive push-pull structured photoinitiators: Indanedione derivatives for radical and cationic photopolymerization reactions. *Macromolecules* **2013**, *46*, 3332–3341. [CrossRef]

49. Tehfe, M.-A.; Dumur, F.; Graff, B.; Morlet-Savary, F.; Gigmes, D.; Fouassier, J.-P.; Lalevée, J. Push-pull (thio)barbituric acid derivatives in dye photosensitized radical and cationic polymerization reactions under 457/473 nm Laser beams or blue LEDs. *Polym. Chem.* **2013**, *4*, 3866–3875. [CrossRef]

50. Xiao, P.; Frigoli, M.; Dumur, F.; Graff, B.; Gigmes, D.; Fouassier, J.-P.; Lalevée, J. Julolidine or fluorenone based push-pull dyes for polymerization upon soft polychromatic visible light or green light. *Macromolecules* **2014**, *47*, 106–112. [CrossRef]

51. Tehfe, M.-A.; Dumur, F.; Graff, B.; Morlet-Savary, F.; Gigmes, D.; Fouassier, J.-P.; Lalevée, J. New push-pull dyes derived from Michler's ketone for polymerization reactions upon visible lights. *Macromolecules* **2013**, *46*, 3761–3770. [CrossRef]

52. Xiao, P.; Dumur, F.; Thirion, D.; Fagour, D.; Vacher, A.; Sallenave, X.; Graff, B.; Fouassier, J.-P.; Gigmes, D.; Lalevée, J. Multicolor photoinitiators for radical and cationic polymerization: Mono vs. poly functional thiophene derivatives. *Macromolecules* **2013**, *46*, 6786–6793. [CrossRef]

53. Xiao, P.; Hong, W.; Li, Y.; Dumur, F.; Graff, B.; Fouassier, J.-P.; Gigmes, D.; Lalevée, J. Green light sensitive diketopyrrolopyrrole derivatives used in versatile photoinitiating systems for photo-polymerizations. *Polym. Chem.* **2014**, *5*, 2293–2300. [CrossRef]

54. Sanguinet, L.; Williams, J.C.; Yang, Z.; Twieg, R.J.; Mao, G.; Singer, K.D.; Wiggers, G.; Petschek, R.G. Synthesis and characterization of new truxenones for nonlinear optical applications. *Chem. Mater.* **2006**, *18*, 4259–4269. [CrossRef]

55. Sigalov, M.V.; Shainyan, B.A.; Chipanina, N.N.; Oznobikhina, L.P. Intra- and intermolecular hydrogen bonds in pyrrolylindandione derivatives and their interaction with fluoride and acetate: Possible anion sensing properties. *J. Phys. Chem. A* **2013**, *117*, 11346–11356. [CrossRef]

56. Feng, H.; Qiu, N.; Wang, X.; Wang, Y.; Kan, B.; Wan, X.; Zhang, M.; Xia, A.; Li, C.; Liu, F.; et al. An A-D-A type small-molecule electron acceptor with end-extended conjugation for high performance organic solar cells. *Chem. Mater.* **2017**, *29*, 7908–7917. [CrossRef]

57. Li, R.; Liu, G.; Xiao, M.; Yang, X.; Liu, X.; Wang, Z.; Ying, L.; Huang, F.; Cao, Y. Non-fullerene acceptors based on fused-ring oligomers for efficient polymer solar cells via complementary light-absorption. *J. Mater. Chem. A* **2017**, *5*, 23926–23936. [CrossRef]

58. Knoevenagel, E. Ueber eine Darstellungsweise des Benzylidenacetessigesters. *Ber. Dtsch. Chem. Ges.* **1896**, *29*, 172–174. [CrossRef]

59. Xiao, P.; Dumur, F.; Zhang, J.; Graff, B.; Morlet-Savary, F.; Fouassier, J.-P.; Gigmes, D.; Lalevée, J. Naphthalic anhydride derivatives: Structural effects on their initiating abilities in radical and/or cationic photopolymerizations under visible light. *J. Polym. Sci. A Polym. Chem.* **2015**, *53*, 2860–2866. [CrossRef]

60. Xiao, P.; Dumur, F.; Zhang, J.; Graff, B.; Gigmes, D.; Fouassier, J.-P.; Lalevée, J. Amino and nitro substituted 2-amino-1*H*-benzo-[*de*]isoquinoline-1,3(2*H*)-diones: As versatile photoinitiators of polymerization from violet-blue LED absorption to a panchromatic behavior. *Polym. Chem.* **2015**, *6*, 1171–1179. [CrossRef]

61. Xiao, P.; Dumur, F.; Zhang, J.; Graff, B.; Gigmes, D.; Fouassier, J.-P.; Lalevée, J. Naphthalimide-phthalimide derivative based photoinitiating systems for polymerization reactions under blue lights. *J. Polym. Sci. A Polym. Chem.* **2015**, *53*, 665–674. [CrossRef]

62. Toba, Y.; Saito, M.; Usui, Y. Cationic photopolymerization of epoxides by direct and sensitized photolysis of onium tetrakis(pentafluorophenyl)borate initiators. *Macromolecules* **1999**, *32*, 3209–3215. [CrossRef]

63. Crivello, J.V.; Lam, J.H.W. Dye-sensitized photoinitiated cationic polymerization. The system: Perylene-triarylsulfonium salts. *J. Polym. Sci. Part A Polym. Chem.* **1979**, *17*, 1059–1065. [CrossRef]

64. Xiao, P.; Dumur, F.; Graff, B.; Morlet-Savary, F.; Gigmes, D.; Fouassier, J.-P.; Lalevée, J. Design of high performance photoinitiators at 385–405 nm: Search around the naphthalene scaffold. *Macromolecules* **2014**, *47*, 973–978. [CrossRef]

65. Dumur, F. Recent advances on pyrene-based photoinitiators of polymerization. *Eur. Polym. J.* **2020**, *126*, 109564. [CrossRef]

66. Xiao, P.; Dumur, F.; Graff, B.; Fouassier, J.-P.; Gigmes, D.; Lalevée, J. Cationic and thiol-ene photopoly-merization upon red lights using anthraquinone derivatives as photoinitiators. *Macromolecules* **2013**, *46*, 6744–6750. [CrossRef]

67. Xiao, P.; Dumur, F.; Graff, B.; Vidal, L.; Gigmes, D.; Fouassier, J.-P.; Lalevée, J. Structural effects in the indanedione skeleton for the design of low intensity 300–500 nm light sensitive initiators. *Macromolecules* **2014**, *47*, 26–34. [CrossRef]

68. Xiao, P.; Dumur, F.; Tehfe, M.-A.; Gigmes, D.; Fouassier, J.-P.; Lalevée, J. Red-light-induced cationic photopolymerization: Perylene derivatives as efficient photoinitiators. *Macromol. Rapid. Commun.* **2013**, *34*, 1452–1458. [CrossRef]

69. Al Mousawi, A.; Arar, A.; Ibrahim-Ouali, M.; Duval, S.; Dumur, F.; Garra, P.; Toufaily, J.; Hamieh, T.; Graff, B.; Gigmes, D.; et al. Carbazole-based compounds as photoinitiators for free radical and cationic polymerization upon near visible light illumination. *Photochem. Photobiol. Sci.* **2018**, *17*, 578–585. [CrossRef]

70. Zhang, J.; Sallenave, X.; Bui, T.-T.; Dumur, F.; Xiao, P.; Graff, B.; Gigmes, D.; Fouassier, J.-P.; Lalevée, J. LED-Induced Polymerization (385, 405, and 455 nm) Using Star-Shaped Tris(4-(thiophen-2-yl)phenyl) amine Derivatives as Light-Harvesting Photoinitiators. *Macromol. Chem. Phys.* **2015**, *216*, 218–227. [CrossRef]

71. Romanczyk, P.P.; Kurek, S.S. The Reduction Potential of Diphenyliodonium Polymerisation Photoinitiator Is Not −0.2 V vs. SCE. A Computational Study. *Electrochim. Acta* **2017**, *225*, 482–485. [CrossRef]

72. Haire, L.D.; Krygsman, P.H.; Janzen, E.G.; Oehler, U.M. Correlation of radical structure with EPR spin adduct parameters: Utility of the proton, carbon-13, and nitrogen-14 hyperfine splitting constants of aminoxyl adducts of PBN-nitronyl-^{13}C for three-parameter scatter plots. *J. Org. Chem.* **1988**, *53*, 4535–4542. [CrossRef]

73. Ohto, N.; Niki, E.; Kamiya, Y. Study of autoxidation by spin trapping. Spin trapping of peroxyl radicals by phenyl *N-t*-butyl nitrone. *J. Chem. Soc. Perkin Trans. 2* **1977**, *13*, 1770–1774. [CrossRef]

74. Dietlin, C.; Schweizer, S.; Xiao, P.; Zhang, J.; Morlet-savary, F.; Graff, B.; Fouassier, J.-P.; Lalevée, J. Photopolymerization upon LEDs: New photoinitiating systems and strategies. *Polym. Chem.* **2015**, *6*, 3895–3912. [CrossRef]

75. Lalevée, J.; Blanchard, N.; Tehfe, M.A.; Morlet-Savary, F.; Fouassier, J.-P. Green bulb light source induced epoxy cationic polymerization under air using *tris*(2, 2′-bipyridine) ruthenium (II) and silyl radicals. *Macromolecules* **2010**, *43*, 10191–10195. [CrossRef]

76. Lalevée, J.; Blanchard, N.; Tehfe, M.A.; Peter, M.; Morlet-Savary, F.; Gigmes, D.; Fouassier, J.-P. Efficient dual radical/cationic photoinitiator under visible light: A new concept. *Polym. Chem.* **2011**, *2*, 1986–1991. [CrossRef]

77. Rehm, D.; Weller, A. Kinetics of fluorescence quenching by electron and H-atom transfer. *Isr. J. Chem.* **1970**, *8*, 259–271. [CrossRef]

78. Zhang, J.; Dumur, F.; Xiao, P.; Graff, B.; Bardelang, D.; Gigmes, D.; Fouassier, J.-P.; Lalevée, J. Structure design of naphthalimide derivatives: Toward versatile photoinitiators for near-UV/visible LEDs, 3D printing, and water-soluble photoinitiating systems. *Macromolecules* **2015**, *48*, 2054–2063. [CrossRef]

79. Xiao, P.; Dumur, F.; Zhang, J.; Fouassier, J.-P.; Gigmes, D.; Lalevée, J. Copper complexes in radical photoinitiating systems: Applications to free radical and cationic polymerization upon visible LEDs. *Macromolecules* **2014**, *47*, 3837–3844. [CrossRef]

80. James, B.; Frisch, A. *Exploring Chemistry with Electronic Structure Methods*; Gaussian Inc.: Wallingford, CT, USA, 1996.

81. Frisch, M.J.; Trucks, G.W.; Schlegel, H.B.; Scuseria, G.E.; Robb, M.A.; Cheeseman, J.R.; Zakrzewski, V.G.; Montgomery, J.A.; Stratmann, R.E.; Burant, J.C.; et al. *Gaussian 03, Revision B-2*; Gaussian Inc.: Pittsburgh, PA, USA, 2003.